Accelerated ions ahead of earthward propagating dipolarization fronts

X.-Z. Zhou,[1] V. Angelopoulos,[1] V. A. Sergeev,[2] and A. Runov[1]

Received 18 March 2010; revised 11 May 2010; accepted 13 May 2010; published 25 September 2010.

[1] We report on the evolving ion distributions associated with the arrival of an earthward propagating dipolarization front in the near-Earth magnetotail using Time History of Events and Macroscale Interactions during Substorms (THEMIS). Ion distributions exhibit steady duskward anisotropy well before the front arrival, suggesting thin current sheet formation at ~11 R_E, during the growth phase of a moderate geomagnetic substorm. As the dipolarization front moves closer, an additional, earthward streaming ion population appears, resulting in an earthward velocity moment. This population eventually overwhelms the preexisting duskward anisotropy and merges with the earthward convecting bulk flow once the dipolarization front arrives. Test-particle simulations show that the observed ion evolution is consistent with a picture of ions reflected and accelerated by the approaching front and moving ahead of it.

Citation: Zhou, X.-Z., V. Angelopoulos, V. A. Sergeev, and A. Runov (2010), Accelerated ions ahead of earthward propagating dipolarization fronts, *J. Geophys. Res.*, *115*, A00I03, doi:10.1029/2010JA015481.

1. Introduction

[2] Transient high-speed plasma flows, known as bursty bulk flows (BBFs), are one of the most important substorm-associated processes carrying significant amounts of mass, energy, and magnetic flux from the reconnection region to the near-Earth magnetotail [*Angelopoulos et al.*, 1994]. It is anticipated that BBFs will be decelerated during their earthward propagation by interacting with the strong magnetic field, which results in magnetic flux pileups in the near-Earth region and eventually produces near-Earth dipolarization [*Hesse and Birn*, 1991; *Shiokawa et al.*, 1997], that is, strong enhancement of the magnetic field component B_z in the magnetotail current sheet.

[3] Recent Time History of Events and Macroscale Interactions during Substorms (THEMIS) observations have shown that the strong B_z enhancement could start very far in the tail and could be very abrupt with typical thickness of several hundred kilometers [*Runov et al.*, 2009; *Sergeev et al.*, 2009]. The sharp dipolarization fronts (DFs), interpreted as vertical thin current sheets embedded within the horizontal tail current sheet [*Sergeev et al.*, 2009], are often observed to be preceded by a minor dip in B_z and followed by a much more gradual B_z decrease [e.g., *Ohtani et al.*, 2004; *Runov et al.*, 2009]. The dipolarization fronts have been also observed to propagate earthward coherently near the leading edge of the fast flows over a distance of ~10 R_E [*Runov et al.*, 2009].

[4] Kinetic simulations [*Sitnov et al.*, 2009] suggest that most of the observed dipolarization signatures, including the steep front, the B_z dip preceding the front, and the gradual B_z decrease that follows it, could be reproduced by transient reconnection in the magnetotail thin current sheet. In the simulations, the entire structure may propagate earthward or tailward from the reconnection region in association with fast flows, which also matches observations.

[5] The interaction of the propagating DFs with the ambient plasma was investigated [*Sergeev et al.*, 2009] by making use of the particle data. In particular, the thin and sharp dipolarization front results in distinct finite gyroradius effects with clear zigzag patterns shown in the azimuthal angular spectra of the ion energy fluxes, from which the DF thickness, orientation, and propagating speed could be determined. Therefore, it is believed that the analysis of particle distributions could provide significant information in diagnosing the properties of the approaching front.

[6] In this paper, another substorm-associated dipolarization event with different ion distribution patterns, that is, the 29 March 2009 event, is studied by using THEMIS observational data [*Angelopoulos*, 2008]. A detailed event description is given in the companion paper (V. A. Sergeev et al., Substorm growth and expansion onset as observed with ideal ground-spacecraft THEMIS coverage, submitted to *Journal of Geophysical Research*, 2010). Here we mainly focus on the evolution of the ion distributions as the dipolarization front propagated toward the near-Earth tail where three THEMIS inner probes (P3, P4, and P5) were located. An approach similar to that of *Zhou et al.* [2009a] is followed by taking advantage of test-particle simulations to reproduce the evolution of the observed ion distributions, which also highlights the importance

[1]Institute of Geophysics and Planetary Physics, University of California, Los Angeles, California, USA.
[2]Institute of Physics, St. Petersburg State University, St. Petersburg, Russia.

0148-0227/10/2010JA015481

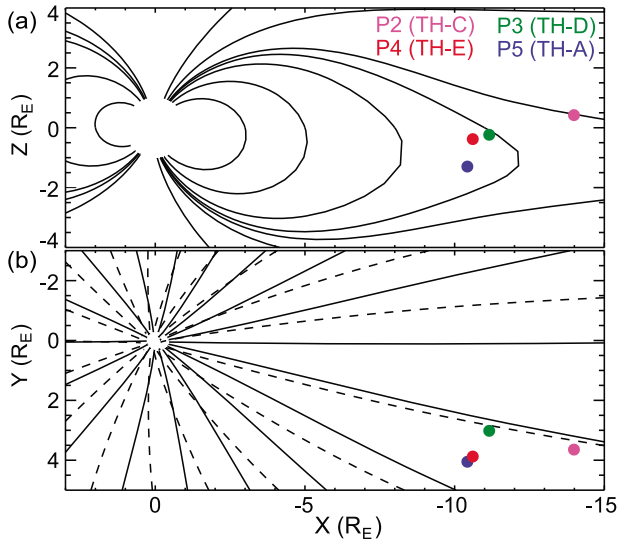

Figure 1. THEMIS P2, P3, P4, and P5 positions at 0517 UT, 29 March 2009, in the GSM (a) *xz* and (b) *xy* planes. Superposed are magnetic field lines obtained from the T96 model [*Tsyganenko*, 1995].

of the particle remote sensing effect on the propagating dipolarization fronts.

2. Observations

[7] In this study, we use observations from the fluxgate magnetometer instrument [*Auster et al.*, 2008], the electrostatic analyzer (ESA) instrument [*McFadden et al.*, 2008], and the solid-state telescope (SST) instrument [*Angelopoulos*, 2008] on board THEMIS. The GSM *xz* and *xy* locations of the THEMIS probes during the 29 March 2009 dipolarization event, at 0517 UT, are shown in Figure 1. It should be noted that the three inner probes (P3, P4, and P5) were clustered in the near-Earth tail with $x \sim -11\ R_E$; that is, P4 was at GSM coordinates $[-10.6, 3.9, -0.4]\ R_E$, with P3 ~1 R_E to the east at $[-11.1, 3.0, -0.2]\ R_E$ and P5 ~1 R_E south at $[-10.4, 4.1, -1.3]\ R_E$.

[8] Figure 2 provides a 3 min overview of the event observed by the THEMIS P3, P4, and P5 probes. At 0516:50 UT, a significant B_z enhancement was observed by P4, indicating the arrival of a dipolarization front. Note that a weaker B_z enhancement was also observed by P2 (located ~3.5 R_E tailward of P4) earlier at 0515:15 UT (not shown), which, according to V. A. Sergeev et al. (submitted, 2010), is the lobe signature of the same reconnection pulse that forms the dipolarization front, and the time delay of ~1.5 min could be used to estimate the propagating speed of the dipolarization front. The estimated speed, ~250 km s^{-1} in the earthward direction, is also consistent with the P4 measurements of the earthward flow velocity as the front arrives.

[9] It is interesting to note that P4 was continuously at the neutral sheet before the front arrival at 0516:50 UT, evidenced by the magnetic field magnitude of ~1–2 nT. The P5 probe, on the other hand, was near the southern lobe, measuring a plasma β of ~0.05 (not shown), which suggests that a taillike magnetic configuration instead of the dipolelike one was present at ~11 R_E. Therefore, the standard T96 model [*Tsyganenko*, 1995], with the predicted field lines shown in Figure 1, may not be accurate at this time during the substorm growth phase (see also V. A. Sergeev et al., submitted, 2010).

[10] Steady azimuthally anisotropic ion fluxes (peaks at ~+90°; valleys at ~−90°) were clearly observed at both P4 and P3 (Figures 2d–2g) prior to 0515:50 UT, suggesting that more ions were moving in the duskward direction. The duskward anisotropy, which actually persisted throughout the entire substorm growth phase and was also observed by P2 and P5 before their exits from the plasma sheet, is expected because of the diamagnetic behavior of ions in the thin current sheet. After that time, and while the dawn-dusk pattern remained, P4 started to observe an additional peak of ion fluxes at ~0° in the earthward direction, which was especially pronounced for energetic ions (30–45 keV) shown in Figure 2d. The peak in the earthward direction, which corresponded to the appearance of the earthward flows (see Figure 2c), coexisted with the preexisting dawn-dusk pattern for around 1 min (until ~0516:50 UT with significant B_z enhancement). After that, the dawn-dusk pattern was overwhelmed by the earthward peak, which was concurrent with the dipolarization front arrival.

[11] Similar features (i.e., the superposition of the dawn-dusk pattern and the peak in the earthward direction) were also observed by P3 during the same time interval. Actually, these signatures are rather common in the THEMIS tail current sheet observations, and similar ion signatures were also observed by Geotail at $X = -10\ R_E$ [see *Angelopoulos et al.*, 1999, Figures 4b and 4f]. It may be interesting to note that our case observations also agree well with statistical surveys of Geotail data, which suggested that earthward flows in the magnetotail (GSM *x* locations between −5 and −31 R_E) typically appear ~2 min before B_z enhancements [*Ohtani et al.*, 2004, Figures 5a and 5b]. Similar results were also obtained in the statistical studies of THEMIS data (T.-S. Hsu et al., manuscript in preparation, 2010).

[12] The observational ion signatures ahead of the earthward propagating dipolarization front, namely, the gradual emergence of an ion angular flux peak in the earthward direction superposed over the preexisting dawn-dusk anisotropy patterns, indicate two things: (1) the earthward flow ahead of the dipolarization front is, to a significant extent, due to a distinct portion of the ion distribution function, and (2) the incoming dipolarization front can affect and precondition the ambient plasma sheet before its arrival.

3. Equilibrium Current Sheet Modeling

[13] We seek to understanding the aforementioned ion signatures ahead of the earthward propagating dipolarization front. Before we start, however, we need to analyze the steady dawn-dusk pattern to determine the population of magnetotail current sheet in the equilibrium state before the earthward peak appearance and the front arrival.

[14] The dawn-dusk anisotropy is caused by the ion diamagnetic motion in the duskward direction, which arises from the pressure gradient either in the earthward direction or toward the neutral sheet [e.g., *Pu et al.*, 1992; *Lee et al.*, 2004]. In the case with negligible B_z component, the diamagnetic motion is more likely to be produced by the pressure gradient in the *z* direction, which was described

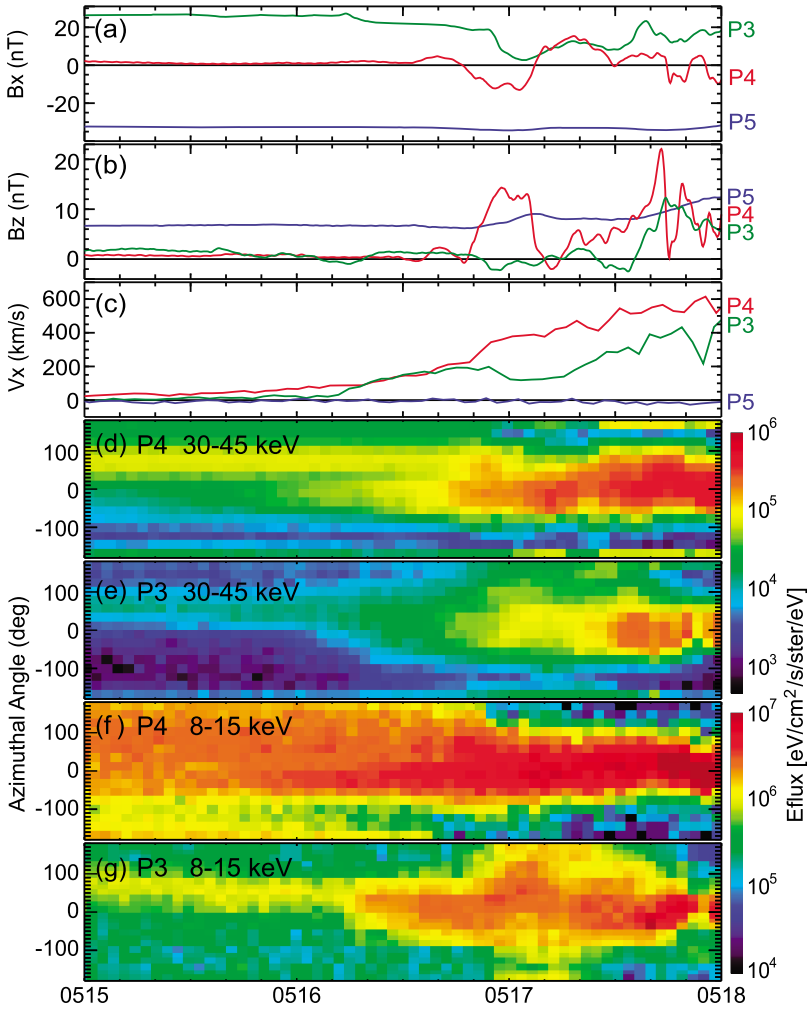

Figure 2. Overview of THEMIS observations during a dipolarization front event on 29 March 2009. GSM magnetic field components (a) B_x and (b) B_z observed by P3, P4, and P5 probes. (c) Plasma flow velocity in the GSM x direction. (d) P4 and (e) P3 ion differential energy fluxes versus azimuth angle in the probe rotation plane, measured by the SST instrument in the 30–45 keV energy range. Here 0° and 90° correspond to the earthward and duskward fluxes, respectively. (f and g) Same format as Figures 2d and 2e, but displaying the spectra in the 8–15 keV range, measured by the ESA instrument.

in the classical *Harris* [1962] model of the current sheet equilibrium. In the Harris model, the duskward diamagnetic drift is naturally obtained by assuming Maxwellian particle distributions with a charge-dependent velocity shift in the y direction (positive for ions and negative for electrons). The shifted Maxwellian distributions could be rewritten as functions of two invariants of motion (the particle energy W and the y component of the canonical momentum P_y), which automatically satisfy the Vlasov equation, and their substitutions to the Maxwell equations would yield a self-consistent solution of the current sheet.

[15] In other words, the entire Harris sheet profile is determined by the assumed particle distributions; for example, the thickness is proportional to the plasma temperature and inversely proportional to the diamagnetic drift velocity. The same is true for other self-consistent current sheet models [e.g., *Schindler and Birn*, 2002; *Yoon and Lui*, 2004; *Sitnov et al.*, 2006; *Liu et al.*, 2010]. Therefore, it becomes possible to obtain the current sheet profiles from single-point observations [*Zhou et al.*, 2009b] by selecting the appropriate model and fitting the observed particle distributions with the modeled ones.

[16] Similar to the work of *Zhou et al.* [2009b], we follow such a procedure in this study to determine the current sheet profile in its equilibrium state well before the dipolarization front arrival, as well as the location-dependent particle distributions within the entire current sheet. On the basis of the fact that three probes (P3, P4, and P5) were clustered with similar x locations, we are able to take advantage of the ion distributions observed at P4 to determine the current sheet profiles, and we compare the P3 and P5 observations with the modeled distributions to check the model accuracy.

[17] Figure 3a shows the ion distribution cut in the yz plane of the spacecraft coordinates observed at P4 at the neutral sheet. Note that, during this time interval, the x direction of the spacecraft coordinates is very close to the GSM x, and the anticlockwise rotation of ~30° in the yz plane could transform the spacecraft coordinates into

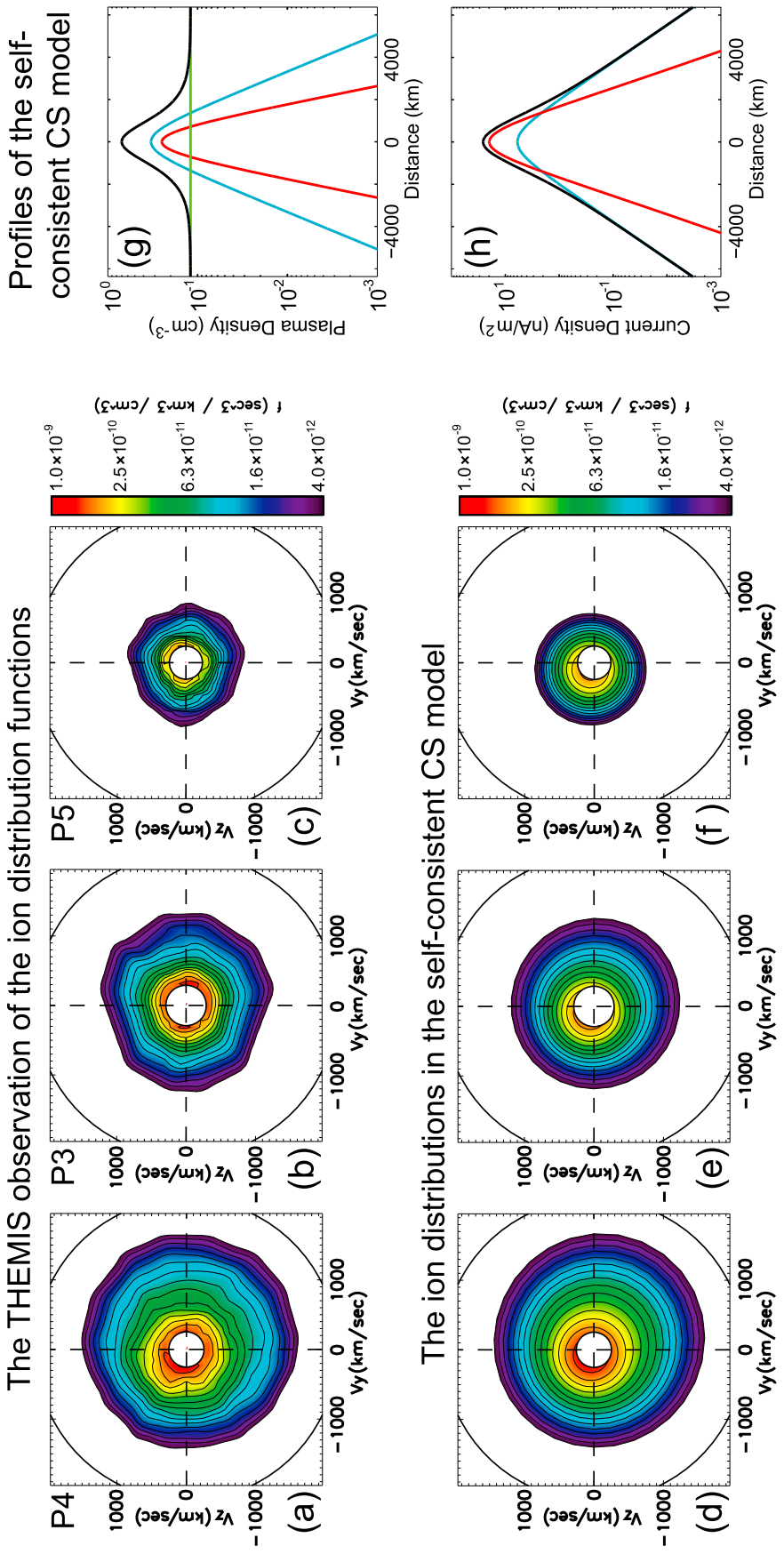

Figure 3. (a) P4, (b) P3, and (c) P5 observations of the ion distribution cuts in the yz plane of the spacecraft coordinates at 0515:40–0515:49 UT, well before the DF arrival at P4. The yz cuts of the ion distributions in the modeled current sheet equilibrium at (d) P4, (e) P3, and (f) P5, with the model parameters derived from a best-fit procedure to match the P4 data. (g) Plasma density profiles of the current sheet model; black line indicates the total density and the green, blue, and red lines correspond to the three plasma components in order of ascending temperature. (h) Same format as Figure 3g, but for the current profiles.

GSM coordinates. It is shown that the ion distribution structure generally shifts in the $+y$ direction, which agrees with the dawn-dusk anisotropy pattern suggested in Figure 2f. However, the observed ion distribution could not be reproduced simply by the Harris-type shifted Maxwellian distributions, because the velocity displacement in the $+y$ direction appears to be energy-dependent, which is more pronounced at higher energy and is actually reversed (in the $-y$ and $+z$ directions) at very low energy. To better reproduce the observed ion distributions, we slightly modify the Harris model by assuming the coexistence of a cold background nondrifting "lobe" plasma component [e.g., *Yoon and Lui* 2004] and two warmer components with different temperatures; the ion distribution function within the equilibrium current sheet becomes

$$f_i = \sum_{\alpha=1}^{3} \frac{N'_\alpha}{\pi^{\frac{3}{2}} v_{Ti\alpha}^3} \exp\left[\frac{2\left(v_{Di\alpha} P_y - W\right)}{m_i v_{Ti\alpha}^2}\right], \quad (1)$$

where subscripts $\alpha = 1, 2, 3$ correspond to the three components with their thermal velocities $v_{Ti\alpha}$ in ascending order. Here N'_α and $v_{Di\alpha}$ are the nominal density and the diamagnetic drift velocity of the ion component α, respectively. Because we have assumed that the coldest ion component is the nondrifting lobe plasma with $v_{Di1} = 0$, the observed velocity displacement in the $-y$ and $+z$ directions at very low energy could be understood as the velocity of the current sheet stationary frame in the P4 coordinates.

[18] At the P4 location of the neutral sheet, with the electric and magnetic potentials both becoming zero, equation (1) degenerates into

$$f_i = \sum_{\alpha=1}^{3} \frac{N_\alpha}{\pi^{\frac{3}{2}} v_{Ti\alpha}^3} \exp\left[\frac{-v_x^2 - \left(v_y - v_{Di\alpha}\right)^2 - v_z^2}{v_{Ti\alpha}^2}\right], \quad (2)$$

where $N_\alpha = N'_\alpha \exp(v_{Di\alpha}^2 / v_{Ti\alpha}^2)$ is the density of the component α at the neutral sheet. A best-fit procedure can thus be performed by minimizing the squared logarithmic differences between equation (2) and the P4 observations to obtain the following parameters: $N_1 = 0.12$ cm^{-3}, $N_2 = 0.33$ cm^{-3}, $N_3 = 0.25$ cm^{-3}, $v_{Ti1} = 370$ km s^{-1}, $v_{Ti2} = 650$ km s^{-1}, $v_{Ti3} = 840$ km s^{-1}, $v_{Di2} = 100$ km s^{-1}, and $v_{Di3} = 360$ km s^{-1}. The best-fit procedure also suggests that the distribution should be rotated clockwise by an angle of 30° in the yz plane of the P4 coordinates, which is the current sheet inclination angle in the P4 coordinates and actually means that the current sheet is purely horizontal in the GSM coordinates given the 30° transformation angle between the GSM and P4 coordinates. Also determined from the procedure is the velocity of the current sheet stationary frame in the P4 coordinates, that is, 80 km s^{-1} in the $-y$ direction and 80 km s^{-1} in the $+z$ direction.

[19] Figure 3d shows the yz cross section of the modeled ion distribution at the P4 location, with the parameters cited earlier. For model completeness, the electron distribution is also assumed to be composed of three shifted Maxwellian components with the density of N_1, N_2, and N_3 at the neutral sheet; the corresponding best-fitted thermal velocities, determined by P4 observations, are $v_{Te1} = 3000$ km s^{-1}, $v_{Te2} = 9800$ km s^{-1}, and $v_{Te3} = 22000$ km s^{-1}. On the basis of the observed electron distributions, however, one can hardly tell the velocity shift $v_{De\alpha}$ for each electron component, because they are much smaller than the corresponding thermal velocities $v_{Te\alpha}$. Here we assume $v_{De\alpha} = -v_{Di\alpha}(m_e v_{Te\alpha}^2 / m_i v_{Ti\alpha}^2)$ to remove the electrostatic field, as was done in the Harris model. Note that the assumption is made for simplicity, and the electrostatic field component E_z may appear if different assumptions on $v_{De\alpha}$ are made in the presence of the background plasma [*Yoon and Lui*, 2004].

[20] The Maxwell equations could now be solved to establish a self-consistent current sheet model. Ion distributions at P3 (~0.2 R_E northward of P4) and P5 (~0.9 R_E southward), shown in Figures 3e and 3f, agree with the observed distributions at those locations seen in Figures 3b and 3c. This confirms that the self-consistent model, despite the additional assumption made with no electrostatic field, is able to satisfactorily describe the ion distributions within the entire current sheet.

[21] The self-consistent plasma and current density profiles of the modeled current sheet are shown in Figures 3g and 3h, respectively. The green, blue, and red lines correspond to the three plasma components in order of ascending temperature, while the black lines represent totals. The modeled current sheet is shown to be very thin, with the plasma and current densities at 2000 km being 26% and 5.5% of the corresponding values at the neutral sheet. Note that the green line in the plasma density profile (Figure 3g) is purely horizontal, and it actually disappears in the current profile (Figure 3h), which comes from the assumption that the coldest component is the nondrifting lobe plasma that carries no current. It is also suggested that the red lines are confined within a thinner layer than the blue lines, which suggests two different scales of the current sheet profiles in the substorm growth phase (see V. A. Sergeev et al., submitted, 2010). These two scales, similar to the case of the Harris model, correspond to the different values between v_{D3}/v_{T3}^2 and v_{D2}/v_{T2}^2.

4. Simulations and Discussions

[22] With the equilibrium current sheet model treated as the initial condition, test-particle simulations can now be carried out to reproduce the observed evolution of the ion distributions (shown in Figures 2d–2f) as the front approaches. As was shown by *Zhou et al.* [2009a], the modeled ion distributions are associated with the ion distributions at later times, on the basis of Liouville's theorem [e.g., *Schwartz et al.*, 1998; *Wanliss et al.*, 2002]. In other words, the ion distributions $f(\mathbf{r}, \mathbf{v}, t)$ at time t can be determined by tracing the ion trajectories backward in time to obtain their initial locations $\mathbf{r}_0$ and velocities $\mathbf{v}_0$ within the modeled equilibrium at t_0 and equating f with the corresponding $f(\mathbf{r}_0, \mathbf{v}_0, t_0)$ values [*Zhou et al.*, 2009a].

[23] Our effort to simulate the evolution of the ion distributions is then constructed based on the computation of ion trajectories in the GSM coordinates. The magnetic field adopted in the trajectory computations is assumed to be the same as the field in the initial equilibrium, except for the superposition of

$$B_z(x,t) = \frac{B_f}{2}\left\{1 - \tanh\left[\frac{x - x_{f0} - v_f(t - t_0)}{L_f}\right]\right\} \quad (3)$$

to model the earthward propagation of a hyperbolic-tangent front at the speed of $v_f = 250$ km s^{-1}. Here $B_f = 10$ nT is the

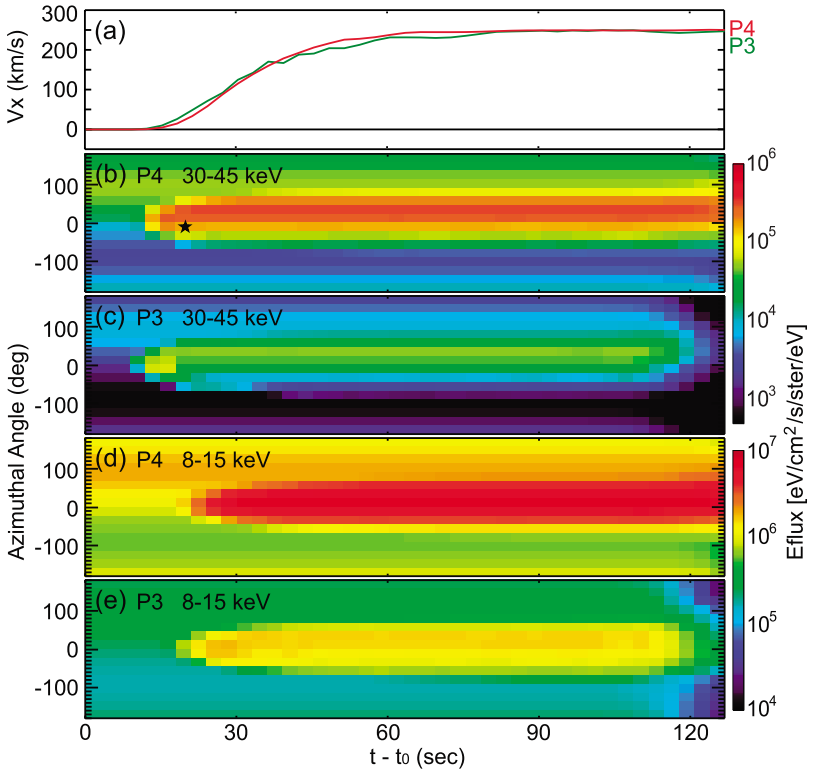

Figure 4. Same format as Figures 2c–2g, but displaying the simulation results of the earthward plasma flow velocities and the ion angular spectra at P4 and P3 locations of the modeled current sheet.

B_z enhancement associated with the DF, L_f = 0.2 R_E is the characteristic DF half thickness, and x_{f0} = −15.6 R_E is the initial DF location (5 R_E tailward of P4 and 1.5 R_E tailward of P2) at $t = t_0$. Note that the dipolarization front arrives at P4 at $t = t_0$ + 127 s (which corresponds to the observational front arrival time of 0516:50 UT), and B_z is generally small at the P4 location until the front becomes very close to P4. Also superposed in the model is a dawn-dusk electric field,

$$E_y(x,t) = v_f B_z, \tag{4}$$

which is built up in accordance with Faraday's law to model the electric field associated with the DF propagation. It should be noted that the aforementioned parameters are determined based on the observational data (see V. A. Sergeev et al., submitted, 2010), which provides a reasonable simplification of the event and therefore enables the computation of ion trajectories to simulate the evolving ion distributions.

[24] The simulation, which stops at $t = t_0$ + 127 s (as the front arrives P4) to avoid taking into account the distinct plasma population behind the front, results in the ion angular spectra shown in Figures 4b–4e. It is found that the earthward peaks, at both P4 and P3 locations, are superposed over the steady dawn-dusk patterns before the front arrival, which are the key signatures of the THEMIS observations shown in Figures 2d–2f. The enhanced earthward ion fluxes also suggest the appearance of the earthward plasma flow ahead of the dipolarization front, as is shown in Figure 4a, with the earthward plasma velocity arising from zero to the front propagating speed of 250 km s^{-1} within ~1 min.

[25] To understand the enhancement of the ion fluxes in the earthward direction, a typical ion trajectory (projected in the GSM *xy* plane) obtained in the simulation is shown in Figure 5a. The ion is selected to reach the P4 location at $t = t_0$ + 20 s (which is 107 s ahead of the DF arrival at P4), with velocity of 300 km s^{-1} in the dawnward direction and 2380 km s^{-1} in the earthward direction (shown as the black

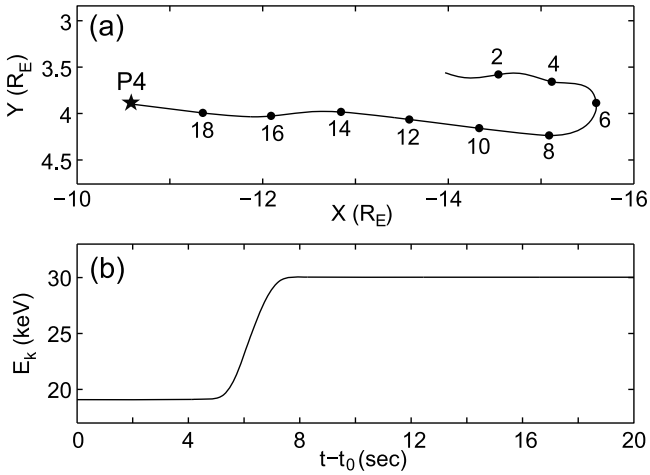

Figure 5. (a) The *xy* projection of a typical ion trajectory (which reaches P4 at $t = t_0$ + 20 s), obtained in the simulation with a dipolarization front propagating earthward. The ion locations at different times are shown by heavy dots, with the numbers nearby indicating the corresponding $t - t_0$ values; (b) kinetic energy of the ion as a function of time.

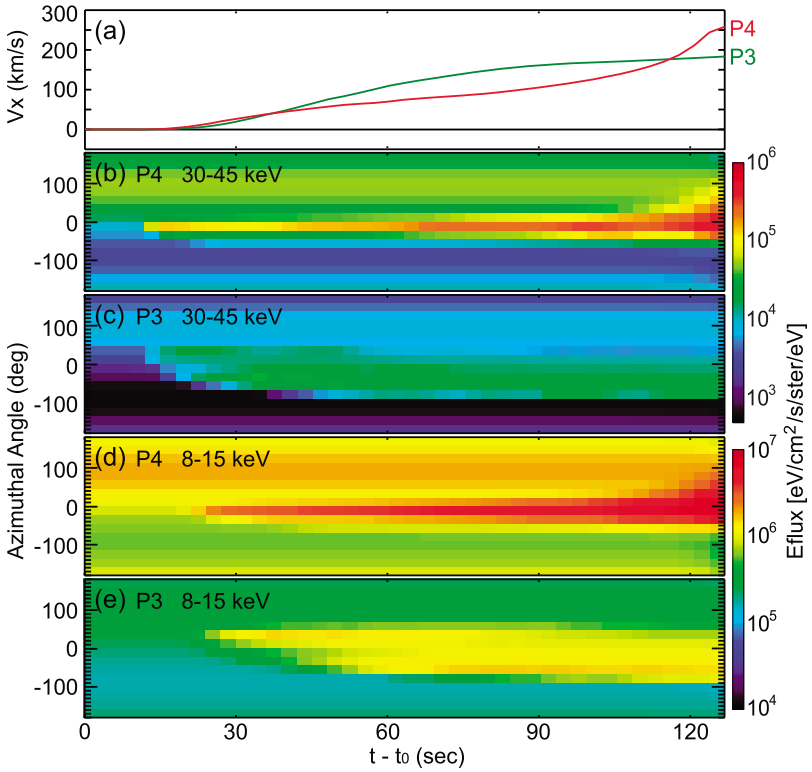

Figure 6. Same format as Figure 4, except that the approaching front in the simulation is localized in the y direction with the characteristic half width of 0.5 R_E.

star in Figure 4b), that is, inside the main earthward moving ion population. Figure 5b shows the kinetic energy of the ion as a function of time.

[26] As is shown in Figure 5, the ion initially moves in the $-x$ direction, and it starts to turn duskward at $t = t_0 + 5$ s when it encounters the approaching front with enhanced B_z values. The gyrating motion lasts ~3 s, which is approximately the ion half gyroperiod in the enhanced B_z field of 10 nT, before the ion eventually returns to the region ahead of the front with negligible B_z field and starts moving in the $+x$ direction. In other words, the ion is reflected earthward by the earthward propagating dipolarization front with energy increased from 19 to 30 keV by the front-associated E_y field (4), which suggests ion acceleration mechanisms very similar the cases in the quasi-parallel bow shock [*Gosling et al.*, 1982; *Scholer et al.*, 1992]. Because the ion energy would be constant in the frame moving with the front (in which E_y disappears), the DF propagating speed of V_f = 250 km s^{-1} suggests that most of the tailward moving ions could be reflected and accelerated by up to 500 km s^{-1} during their DF encounters, which agrees with the ion energy enhancement shown in Figure 5b from 19 keV (with a speed of 1900 km s^{-1}) to 30 keV (or 2400 km s^{-1}).

[27] The ion reflection and acceleration mechanism, however, may provide an additional way to decelerate the incoming front, and the relative importance of this deceleration mechanism could be approximately estimated. Considering the frame moving with the dipolarization front, the ion reflection effect could be treated as a dynamic pressure of $2Nm_iv_f^2$ imposed on the front, in analogy with the classical Chapman-Ferraro problem of the pressure balance on the magnetopause. In this case, with N = 0.7 cm^{-3} and v_f = 250 km s^{-1}, the equivalent dynamic pressure could be calculated as 0.15 nPa, which is around 40% of the plasma thermal pressure at the neutral sheet (observed by P4) before the front arrival and therefore suggests that the deceleration mechanism is not negligible.

[28] The major differences between the simulations and the THEMIS observations, however, are the relatively higher values of the earthward ion fluxes in the simulations (especially in Figure 4b compared with Figure 2d), along with their earlier appearances (nearly 2 min ahead of the front arrival in the simulations in comparison with ~1 min in the observations). The less enhanced ion fluxes in the observations may be due to the limited y scale of the real dipolarization front, which suggests that only some of the ions observed in the earthward direction were accelerated by the localized front. Here we consider a case with the B_z field (3) and the E_y field (4) adopted in the previous simulation, both multiplied by a Gaussian function $G(y) = \exp[-(y - y_0)^2/H_f^2]$, to model the approach of a localized dipolarization front with Faraday's law remaining satisfied. The approaching front, centered at $y_0 = 4.0\ R_E$ with a characteristic half width of $H_f = 0.5\ R_E$, which is consistent with the observations (shown in Figure 2b) that the strong B_z enhancement was recorded at P4 but not at P3, results in the simulated plasma velocity V_x and ion angular spectra shown in Figure 6.

[29] It is clear that both the earthward streaming ion fluxes and the V_x values are less enhanced (than those in Figure 4), which better agrees with the observations. Although the timing discrepancies in which the earthward ion fluxes appear earlier in the simulations than in the observations are

hardly resolved in this case, the introduction of the localized dipolarization front may still have the potential to explain the timing differences, given the strong dependence of the earthward ion fluxes on the location and width of the approaching front, because the THEMIS probes may not always be at the correct *y* location to observe the ion reflected and accelerated by the localized front.

[30] Another possible explanation may arise from the assumed *x* and *y* independence of the initial equilibrium. In a more realistic case with the current sheet ion density decreasing as the distance from the Earth increases, the more tenuous ions initially located closer to the front (at smaller *x* locations) would be accelerated first, resulting in the observed lower values of the earthward ion fluxes.

[31] Despite the differences, even the simplified simulations could reproduce the essential features of the observations, suggesting that the approaching DF could be remotely sensed by accelerated ions in the observations of ion distributions. The information contained in the observed ion distributions, however, is not yet fully exploited, and it is our goal to further develop our reconstruction technique to arrive at a better understanding of the origin, propagation, and evolution of these structures.

5. Summary

[32] Evolving ion distributions in association with the approach of an earthward propagating dipolarization front during the 29 March 2009 substorm event were studied. We concentrated on the gradual emergence of an ion angular flux peak in the earthward direction superposed on the steady dawn-dusk anisotropy patterns. Using the tail current sheet structures as determined by analyzing the preexisting dawn-dusk patterns, test-particle simulations were performed to reproduce the key features of the observed ion distributions. The similarities between the simulations and the observations well support the idea that the ions were reflected and accelerated by the approaching front and moved earthward in the DF upstream region. It is suggested that the incoming front could be decelerated by these reflected ions, and the same mechanism could also precondition the ambient plasma sheet before the front arrival. This preconditioning means that significant information regarding the approaching front could be remotely sensed by the observations of particle distributions, and it highlights the importance of extracting such information in the study of earthward propagating front structures.

[33] **Acknowledgments.** The work was supported by NASA grant NAS5-02099, and the work by V.S. was supported by RFBR grants 10-05-00223 and 10-05-91163. The authors are grateful to M. I. Sitnov, Q.-G. Zong, Z. Y. Pu, M. Fujimoto, T.-S. Hsu, and Y. S. Ge for valuable discussions and suggestions.

[34] Masaki Fujimoto thanks the reviewers for their assistance in evaluating this manuscript.

References

Angelopoulos, V. (2008), The THEMIS mission, *Space Sci. Rev.*, *141*, 5–34, doi:10.1007/s11214-008-9336-1.

Angelopoulos, V., et al. (1994), Statistical characteristics of bursty bulk flow events, *J. Geophys. Res.*, *99*, 21,257–21,280, doi:10.1029/94JA01263.

Angelopoulos, V., F. S. Mozer, T. Mukai, K. Tsuruda, S. Kokubun, and T. J. Hughes (1999), On the relationship between bursty flows, current disruption and substorms, *Geophys. Res. Lett.*, *26*, 2841–2844, doi:10.1029/1999GL900601.

Auster, H. U., et al. (2008), The THEMIS Fluxgate Magnetometer, *Space Sci. Rev.*, *73*, 235–264, doi:10.1007/s11214-008-9365-9.

Gosling, J. T., M. F. Thomsen, S. J. Bame, W. C. Feldman, G. Paschmann, and N. Sckopke (1982), Evidence for specularly reflected ions upstream from the quasi-parallel bow shock, *Geophys. Res. Lett.*, *9*, 1333–1336, doi:10.1029/GL009i012p01333.

Harris, E. G. (1962), On a plasma sheath separating regions of oppositely directed magnetic field, *Nuovo Cimento*, *23*, 115.

Hesse, M., and J. Birn (1991), On dipolarization and its relation to the substorm current wedge, *J. Geophys. Res.*, *96*, 19,417–19,426, doi:10.1029/91JA01953.

Lee, E., M. Wilber, G. K. Parks, K. W. Min, and D.-Y. Lee (2004), Modeling of remote sensing of thin current sheet, *Geophys. Res. Lett.*, *31*, L21806, doi:10.1029/2004GL020331.

Liu, W. W., J. Liang, and E. F. Donovan (2010), Electrostatic field and ion temperature drop in thin current sheets: A theory, *J. Geophys. Res.*, *115*, A03211, doi:10.1029/2009JA014359.

McFadden, J. P., C. W. Carlson, D. Larson, M. Ludlam, R. Abiad, B. Elliott, P. Turin, M. Marckwordt, and V. Angelopoulos (2008), The THEMIS ESA plasma instrument and in-flight calibration, *Space Sci. Rev.*, *141*, 277–302, doi:10.1007/s11214-008-9440-2.

Ohtani, S., M. A. Shay, and T. Mukai (2004), Temporal structure of the fast convective flow in the plasma sheet: Comparison between observations and two-fluid simulations, *J. Geophys. Res.*, *109*, A03210, doi:10.1029/2003JA010002.

Pu, Z. Y., A. Korth, and G. Kremser (1992), Plasma and magnetic field parameters at substorm onsets derived from GEOS 2 observations, *J. Geophys. Res.*, *97*, 19,341–19,349, doi:10.1029/92JA01732.

Runov, A., V. Angelopoulos, M. I. Sitnov, V. A. Sergeev, J. Bonnell, J. P. McFadden, D. Larson, K. Glassmeier, and U. Auster (2009), THEMIS observations of an earthward-propagating dipolarization front, *Geophys. Res. Lett.*, *36*, L14106, doi:10.1029/2009GL038980.

Schindler, K., and J. Birn (2002), Models of two-dimensional embedded thin current sheets from Vlasov theory, *J. Geophys. Res.*, *107*(A8), 1193, doi:10.1029/2001JA000304.

Scholer, M., K. J. Trattner, and H. Kucharek (1992), Ion injection and Fermi acceleration at Earth's bow shock—The 1984 September 12 event revisited, *Astrophys. J.*, *395*, 675–681, doi:10.1086/171687.

Schwartz, S. J., P. W. Daly, and A. N. Fazakerley (1998), Multi-spacecraft analysis of plasma kinetics, in *Analysis Methods for Multi Spacecraft Data*, edited by G. Paschmann and P. W. Daly, pp. 159–184, European Space Agency, Bern, Switzerland.

Sergeev, V. A., V. Angelopoulos, S. Apatenkov, J. Bonnell, R. Ergun, R. Nakamura, J. P. McFadden, D. Larson, and A. Runov (2009), Kinetic structure of the sharp injection/dipolarization front in the flow-braking region, *Geophys. Res. Lett.*, *36*, L21105, doi:10.1029/2009GL040658.

Shiokawa, K., W. Baumjohann, and G. Haerendel (1997), Braking of high-speed flows in the near-Earth tail, *Geophys. Res. Lett.*, *24*, 1179–1182, doi:10.1029/97GL01062.

Sitnov, M. I., M. Swisdak, P. N. Guzdar, and A. Runov (2006), Structure and dynamics of a new class of thin current sheets, *J. Geophys. Res.*, *111*, A08204, doi:10.1029/2005JA011517.

Sitnov, M. I., M. Swisdak, and A. V. Divin (2009), Dipolarization fronts as a signature of transient reconnection in the magnetotail, *J. Geophys. Res.*, *114*, A04202, doi:10.1029/2008JA013980.

Tsyganenko, N. A. (1995), Modeling the Earth's magnetospheric magnetic field confined within a realistic magnetopause, *J. Geophys. Res.*, *100*, 5599–5612, doi:10.1029/94JA03193.

Wanliss, J. A., R. D. Sydora, G. Rostoker, and R. Rankin (2002), Origin of some anisotropic tailward flows in the plasma sheet, *Ann. Geophys.*, *20*, 1559–1575.

Yoon, P. H., and A. T. Y. Lui (2004), Model of ion- or electron-dominated current sheet, *J. Geophys. Res.*, *109*, A11213, doi:10.1029/2004JA010555.

Zhou, X.-Z., V. Angelopoulos, A. Runov, M. I. Sitnov, Q.-G. Zong, and Z. Y. Pu (2009a), Ion distributions near the reconnection sites: Comparison between simulations and THEMIS observations, *J. Geophys. Res.*, *114*, A12211, doi:10.1029/2009JA014614.

Zhou, X.-Z., et al. (2009b), Thin current sheet in the substorm late growth phase: Modeling of THEMIS observations, *J. Geophys. Res.*, *114*, A03223, doi:10.1029/2008JA013777.

V. Angelopoulos, A. Runov, and X.-Z. Zhou, Institute of Geophysics and Planetary Physics, University of California, 3845 Slichter Hall, Los Angeles, CA 90095, USA. (xzhou@igpp.ucla.edu)

V. A. Sergeev, Institute of Physics, St. Petersburg State University, Ulyanovskya 1, St. Petersburg 198504, Russia.